

Effect of hydrostatic pressure on transport in the topological insulator $\text{Bi}_2\text{Te}_2\text{Se}$

Yongkang Luo^{1,2}, Stephen Rowley^{1,*}, Jun Xiong¹, Shuang Jia³, R. J. Cava³, and N. P. Ong¹

¹*Department of Physics, Princeton University, Princeton, New Jersey 08544, U.S.A.*

²*Department of Physics, Zhejiang University, Hangzhou 310027, P. R. China.*

³*Department of Chemistry, Princeton University, Princeton, New Jersey 08544, U.S.A*

(Dated: August 14, 2018)

The Hall coefficient R_H and resistivity ρ of the topological insulator $\text{Bi}_2\text{Te}_2\text{Se}$ display a number of puzzling features vs. temperature T . We propose a model that describes well the non-monotonic variation of $R_H(T)$. A key feature of the model is a chemical potential that is weakly T -dependent. From the fit to the model, we infer a “transport” gap Δ_T of 50 mV. We find that hydrostatic pressure P (0-27 kbar) has a pronounced effect on both R_H and ρ . We show that these changes arise from decreases in both Δ_T and the hole effective mass under pressure.

PACS numbers: 74.62.Fj, 73.20.At, 72.20.-i, 73.25.+i

Topological Insulators are a class of semiconductors in which the bulk energy gap is traversed by current-carrying surface states, which have a massless, Dirac dispersion. A novel feature of the surface state is the locking of the spin of the surface electron perpendicular to its momentum with a helicity that has opposite signs on opposing faces of a crystal [1–6]. The spin locking strongly suppresses back-scattering. In several Bi-based semiconductors, the existence of the topological surface state (SS) and its spin-locked nature have been established by angle-resolved photoemission spectroscopy (ARPES) [7–10]. Detailed scanning tunneling microscopy (STM) experiments have also confirmed the spin-locked nature of the surface states [11]. In transport experiments, Shubnikov-de Haas (SdH) oscillations from the SS have been detected in Bi_2Te_3 [14], and in $(\text{Bi,Sb})_2\text{Se}_3$ [15]. Analysis of the SdH oscillations in Bi_2Te_3 [14] yields a surface mobility $\mu_s = 8,000\text{--}10,000 \text{ cm}^2/\text{Vs}$. Despite the high mobility, the bulk conductance G_b can exceed the surface conductance G_s by factors of 3000 or more in crystals of these materials. A major experimental task is to bring the ratio G_b/G_s significantly below 1.

Recently, the hybrid semiconductor $\text{Bi}_2\text{Te}_2\text{Se}$ has emerged as a highly promising topological insulator (TI) for transport experiments [16, 17]. ARPES measurements [18] reveal a single spin-locked Dirac state crossing a bulk energy gap of ~ 350 mV. The Dirac point lies close to the top of the bulk valence band at the Γ point. In carefully annealed crystals, the observed resistivity ρ at 4 K (Fig. 1) is typically $1 \text{ }\Omega\text{cm}$, but can be much larger. In Refs. [17, 19], we show that in crystals with $\rho(4 \text{ K}) = 6 \text{ }\Omega\text{cm}$, the surface SdH oscillations are especially well-resolved. The surface SdH oscillations yield a surface mobility $\mu_s = 2,800\text{--}3,200 \text{ cm}^2/\text{Vs}$, which implies that the ratio G_b/G_s is ~ 1 . At 4 K, the residual bulk carriers are n -type with a bulk density n_b equal to $\sim 3 \times 10^{16} \text{ cm}^{-3}$ (compared with $10^{18}\text{--}10^{19} \text{ cm}^{-3}$ in Bi_2Te_3 and Bi_2Se_3). Hall measurements show that the bulk mobility μ_b is 60 times smaller than μ_s at 4 K [16, 17].

Despite the large ρ in $\text{Bi}_2\text{Te}_2\text{Se}$, much of its bulk conduction features are puzzling. The Hall coefficient R_H displays an interesting non-monotonic profile vs. T that seems unrelated to thermal activation at first glance (Fig. 2). To further improve the quality of $\text{Bi}_2\text{Te}_2\text{Se}$ crystals, a better understanding

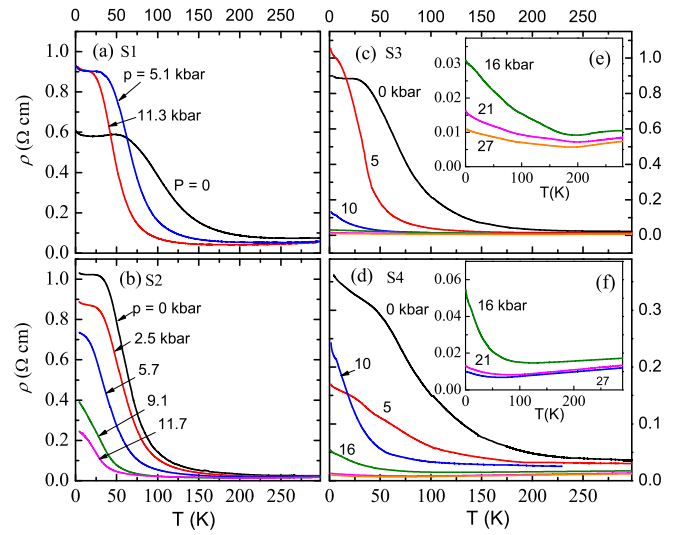


FIG. 1: (Color online) The resistivity profiles, ρ vs. T , at selected pressures in $\text{Bi}_2\text{Te}_2\text{Se}$ for samples S1...S4 (Panels a...d, respectively). Resistivities of Samples S3 and S4 at higher P are shown in Panels (e) and (f), respectively. In sample S1, the curves were measured in the sequence $P = 0, 11.3$ and 5.1 kbar. In all panels, ρ is plotted along the vertical axes, and T along the horizontal axes.

of where the bulk carriers come from is clearly important. We propose a model that accounts well for the T dependence of the weak-field conductivity tensor. We show that the transport quantities are consistent with thermal activation across a small transport gap of ~ 50 mV. A key feature of the model is a weakly T -dependent chemical potential $\mu(T)$. Hydrostatic pressure allows us to tune the system parameters. We show that the observed changes are consistent with the model. In addition, we uncover an interesting trend under pressure in the magnetoresistance.

Four crystals of $\text{Bi}_2\text{Te}_2\text{Se}$, grown by a modified Bridgman method [16, 17] (Samples S1...S4), were investigated. Two piston-cylinder pressure cells were used, with high-purity Pb or Sn serving as the manometer. The pressure was determined

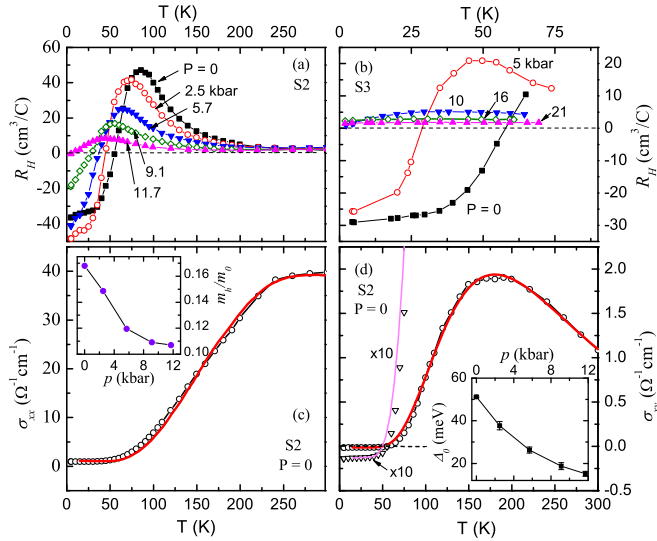


FIG. 2: (Color online) The temperature dependence of the Hall coefficient R_H in samples S2 (Panel a) and S3 (Panel b) at the pressures indicated. The solid curves in (a) and (b) are guides to the eye. Panels (c) and (d) plot the conductivity σ_{xx} and Hall conductivity σ_{xy} derived from R_H and ρ in S2 at $P = 0$ (open symbols). The bold curves are the fits of the data to the proposed model. In Panel (d), we replot for clarity the low- T data (triangles) and the fit (thin curve) in expanded scale ($\times 10$). The effective mass m_h and transport gap $\Delta_T(0) = \Delta_0$ derived from the fits in S2 are plotted vs. P in the insets in Panels (c) and (d), respectively.

by the pressure-dependent superconducting transition temperature of Pb (or Sn), as well as the resistance ratio $R(p)/R(0)$ at room temperature. Thin crystals with mirror-like surfaces (nominally $1.5 \times 0.6 \times 0.02$ mm in size) were cleaved from the ingot. The cleaved faces expose the outer Te layers. The axes **a** and **b** lie in the layer, and the axis **c** is normal to the cleavage plane. Ohmic contacts were made in the Hall-bar configuration on each crystal. With daphne oil as the pressure fluid, we attained a maximum hydrostatic pressure of 27 kbar.

Figure 1 plots the temperature dependence of ρ under pressure. At ambient pressure ($P = 0$), the observed resistivity ρ initially increases steeply as the temperature T is decreased from 300 K, but tends towards a plateau value below 50 K. This saturation implies a parallel metallic conduction channel that has been identified to be the topological surface states [16, 17]. With applied pressure, the ρ - T profile generally becomes much more metallic at all T . We observe two classes of behavior. In S2, ρ at 4 K decreases monotonically with increasing P (Fig. 1b), whereas, in S1, S3 and S4, the change is non-monotonic if $P < 10$ kbar (Panels a, c and d). However, above 10 kbar, $\rho(T)$ tends towards a metallic profile with a weak T dependence in all samples.

Pressure also has a pronounced effect on the Hall coefficient R_H , as shown in Fig. 2a (in S2) and Fig. 2b (S3). At $P = 0$, the curve R_H vs. T in S2 displays a characteristic peak at 80 K and a zero-crossing at 58 K [16]. In applied pressure, both features shift monotonically to lower T . Simultaneously, the large negative plateau at low- T moves upwards, eventually

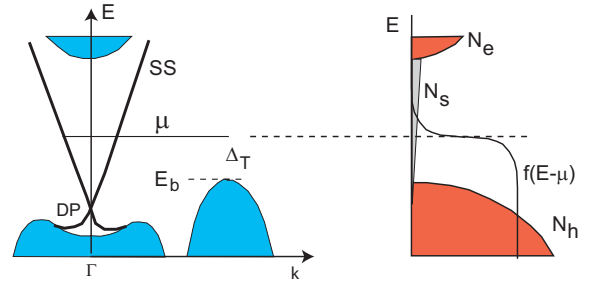


FIG. 3: (Color online) Sketch of the band structure near the Γ point. The left panel shows the Dirac surface state (SS) as bold lines. The chemical potential μ lies ~ 130 mV above the Dirac point (DP). Shaded regions represent bulk bands. The maximum of the valence band lies below μ by the energy spacing Δ_T (the maximum is likely at a finite \mathbf{k}). The fits show that μ is T dependent. The right panel shows the densities of states of the bulk conduction and hole bands (N_e and N_h , respectively) and the surface states N_s . The solid curve labelled as $f(E - \mu)$ is the Fermi-Dirac distribution.

attaining a positive value at 11.7 kbar. For S3, R_H is already positive at all T at 10 kbar. To exploit the additivity of the conductivities, we invert the resistivity tensor ρ_{ij} to obtain the conductivity tensor σ_{ij} . The inferred conductivity σ_{xx} and Hall conductivity σ_{xy} are plotted as open circles in Panels (c) and (d), respectively. Also plotted are the fits (bold curves) to these quantities using the following model.

As may be seen in the expanded scale in Panel (d), σ_{xy} (open triangles) is negative and nearly T -independent below 30 K. Above 30 K, σ_{xy} undergoes an exponential increase to very large positive values. This suggests that we have a small density of n -type carriers at low T , which are overwhelmed by a divergent population of holes induced by thermal activation across a small gap. However, because σ_{xy} rises to a broad peak at 180 K, the exponential growth is eventually tempered by high- T processes.

TABLE I: Fit parameters at selected pressures P (for Sample S2). Δ_0 is the transport gap at $T = 0$, γ the coefficient of the T^2 term in the gap, m_h the hole effective mass (with m_0 the free electron mass) and β is the exponent in the hole mobility.

P (kbar)	Δ_0 (meV)	γ (meV/K ²)	m_h/m_0	β
0	51	6.30×10^{-4}	0.168	1.79
2.5	38	7.70×10^{-4}	0.149	0.86
5.7	26	7.52×10^{-4}	0.119	0.71
9.1	19	7.17×10^{-4}	0.109	0.76
11.7	15	5.76×10^{-4}	0.107	1.30

At 4 K, we assume that charge conduction involves carriers in the topological surface state and a dilute concentration of bulk carriers (both n -type). As found in Ref. [17], the bulk carriers, which have very low mobility ($\mu_b \sim 50$ cm²/Vs), occupy an impurity band. By contrast, the high mobility of the surface electrons ($\mu_s \sim 3,000$ cm²/Vs) leads to SdH oscillations (see below). The data at 4 K, restricted to relatively low

B , do not allow the surface and bulk electrons to be separated (in Refs. [14, 17], the separation was accomplished by using the SdH oscillation amplitudes), we treat the two bands here as one band with an effective mobility $\mu_e = A/(1 + CT^\alpha)$, with α , A and C as free parameters.

The conductivity is $\sigma_{xx} = 2e^2 \sum_{\mathbf{k}} (-\partial f / \partial E) v_x(\mathbf{k})^2 \tau$, where $f(E - \mu)$ is the Fermi-Dirac distribution, $\mathbf{v}(\mathbf{k})$ the group velocity at the wavevector \mathbf{k} and τ is the transport lifetime. With the chemical potential μ in the bulk gap as sketched in Fig. 3, we obtain for the holes $\sigma_{xx} = n_h e \mu_h$ and $\sigma_{xy} = n_h e \mu_h^2 B$, with μ_h the hole mobility. In the limit $\Delta_T / k_B T \gg 1$ (k_B is the Boltzmann constant) the hole population has the activated form

$$n_h(T) = \frac{1}{4} \left(\frac{2m_h k_B T}{\pi \hbar^2} \right)^{\frac{3}{2}} e^{-\Delta_T / k_B T}, \quad (1)$$

where m_h is the hole effective mass. The energy scale $\Delta_T \equiv \mu - E_b$ is the ‘‘transport gap’’ that dictates the exponential growth in σ_{xy} at low T (E_b is the energy at the valence band maximum). As we show below, we may ignore thermal activation to the conduction band for $T < 300$ K. We express the hole mobility as $\mu_h = DT^{-\beta}$, with D and β as free parameters (the impurity scattering rate for the holes plays no role in the fitting because the holes are thermally activated).

To fit the data at high T , however, we further assume that Δ_T has the temperature dependence

$$\Delta_T(T) = \Delta_0 + \gamma T^2, \quad (2)$$

with Δ_0 and γ as free parameters.

The fits to the conductivity tensor are plotted as bold curves in Figs. 2c and 2d. We remark that our primary goal is to describe the weak-field hole conductivity tensor using the 4 constants Δ_0 , γ , m_h and β . The strong thermal activation at low T and the pronounced non-monotonicity of σ_{xy} at high T severely restrict the physically reasonable values that these parameters may assume. Hence the convergence of the fits is rapid and relatively unambiguous (by contrast, the n -band parameters α , A and C are less reliably obtained because the n -type carriers are resolved only below 30 K). We have extended the fits to finite P as well for S2. The optimal parameters are reported in Table I.

From the fits, we infer that the steep exponential increase in σ_{xy} when T is raised above 30 K (triangles in Fig. 2d) results from the thermal activation of holes into the valence band (Eq. 1). The monotonic decrease of the hole mobility μ_h with increasing T tends to counter this increase, especially in $\sigma_{xy} \sim \mu_h^2$. However, to produce the non-monotonic variation in σ_{xy} , we need Δ_T to increase slightly with T as in Eq. 2. We attribute this increase to a T -dependent chemical potential. Particle number conservation dictates that μ must change with T when $k_B T$ is large enough to reach a band with a large density of states (here the hole band). This causes μ to move away from the valence band with an increment varying as T^2 . At ambient P , the increment is 6.3 mV when $T = 100$ K (Table I). As a consequence, $n_h(T)$ grows much more slowly above 200 K, resulting in an overall decrease in σ_{xy} as observed. We expect a T -dependent μ to be a general feature in topological insulators because μ lies close to one of the bulk band extrema.

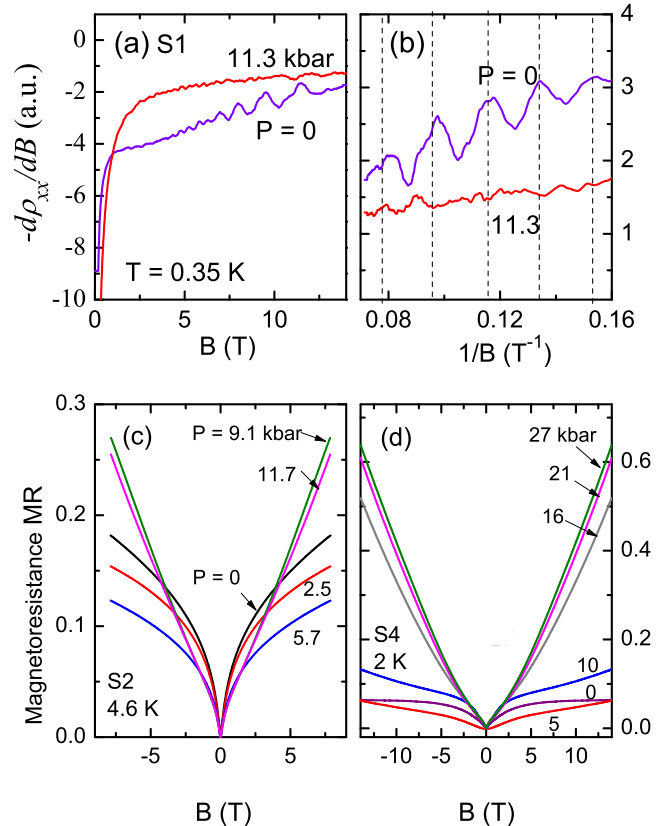


FIG. 4: (Color online) Comparison of the magnetoresistance curves at ambient pressure and high pressure. In Panel (a), the derivative $d\rho_{xx}/dB$ at $P = 0$ and $T = 0.35$ K displays SdH oscillations from the surface states. Panel (b) shows that the oscillations are periodic in $1/B$, with a period that yields $k_F = 0.040 \text{ \AA}^{-1}$. The oscillations become unresolved at 11.7 kbar. In Panels (c) and (d), we plot the MR curves (measured with $\mathbf{B} \parallel \mathbf{c}$) at selected pressures for Samples S2 (at 4.6 K) and S4 (2 K), respectively. In both samples, the MR changes from a saturation trend (at low P) to one that is large and quadratic in B at large P .

As in Refs. [14, 16, 17], we may estimate the position of μ by detecting the weak surface SdH oscillations (Fig. 4a). From the period of the oscillations at 0.35 K, we obtain the surface Fermi wavevector $k_F = 0.040 \text{ \AA}^{-1}$. Using the surface Fermi velocity $v_F = 6 \times 10^5 \text{ m/s}$ [17, 18], the k_F value implies that μ lies 130 mV above the Dirac point. ARPES [18] shows that the direct gap at the Γ point ($\mathbf{k} = \mathbf{0}$) is 350 mV. Hence the conduction band minimum lies 220 mV above μ . As this separation exceeds Δ_T by a factor of ~ 4 , we are justified in ignoring thermal excitations into the conduction band. In addition, we note that Δ_T is quite small compared to the spacing of μ from the Dirac point (130 mV). This implies that the valence-band maximum is at a finite \mathbf{k} , as drawn in Fig. 3.

From the fits, we now see that the dramatic effect of P on the transport properties stems primarily from the steep de-

crease of the transport gap. In Sample S2 (inset in Fig. 2d), the zero-Kelvin value Δ_0 decreases from 51 mV (at $P = 0$) to 15 mV ($P = 11.7$ kbar). Thus, at 11.7 kbar, the smallness of Δ_0 results in a large population of excited holes even at 4 K (R_H is close to zero at 11.7 kbar). Nonetheless, a vestige of the activated behavior can be seen at 11.7 kbar in ρ vs. T (Fig. 1c). At larger P (16-27 kbar), Δ_T is nearly completely suppressed (Fig. 1d, for S4), and the system remains p type down to 4 K. In addition, the fits reveal that an increasing P decreases the hole effective mass from 0.16 times the free mass (at $P = 0$) to 0.11 (at 11.7 kbar). The most significant effect, however, is that increasing P suppresses the surface conductance, rendering it difficult to resolve against the increased hole conduction. Direct evidence for this suppression is obtained by comparing the curves of $d\rho_{xx}/dB$ (Fig. 4a,b). The prominent SdH oscillations at $P = 0$ become unresolved at 11.3 kbar. Thus, in closing the transport gap, pressure converts the system from a TI in which surface conductance G_s is easily observed at 0.35 K to one that is dominated by the bulk holes.

Tuning the relative weights of G_s and G_b by pressure provides a powerful way to separate transport characteristics of the surface states from bulk states. As an example, we examine the transverse magnetoresistance, defined as the fractional change in $\rho(B)$, viz. $MR(B) = [\rho(B)/\rho(0)] - 1$, measured with $\mathbf{B}||\mathbf{c}$. Figures 4c and 4d plot the curves of $MR(B)$ at several pressures for Samples S2 (at 4.6 K) and S4 (at 2 K), respectively. In both samples, when G_s and G_b are comparable (at low P), the MR tends towards saturation at large fields. However, when G_b dominates (large P), the MR switches to a quadratic variation ($\sim B^2$) consistent with the semiclassical

MR observed for bulk states in a high-mobility semi-metal. In both samples, the dominance of the bulk conduction at large P is again evident in the large, semi-classical B^2 variation of ρ . Currently, there is very little understanding of the MR of both the bulk and surface states, as discussed in Ref. [14]. The present results suggest that the behavior of the MR with pressure tuning may reveal specific characteristics of the topological surface state, and provide a way to readily distinguish surface from bulk conduction.

Finally, we remark that the fits provide a clearer picture of the overall band structure in crystals of $\text{Bi}_2\text{Te}_2\text{Se}$ that have μ inside the bulk gap. We obtain an accurate determination of the gap $\Delta_T(T)$, which dictates the bulk carrier concentration above 30 K, as well as its sensitivity to applied pressure. It should be instructive to see how these numbers are altered when the pure compound is doped with donors or acceptors. An interesting test of the inferred band alignments may be made with thermopower, which is sensitive to the band parameters.

We acknowledge support from the National Science Foundation under Grant DMR 0819860 and from the Nano Electronics Research Corporation (Award 2010- NE-2010G). Y.K.L. acknowledges a scholarship given by the China Scholarship Council (CSC).

**Current affiliations of SR:* Centre for Materials and Microsystems, Fondazione Bruno Kessler, I-38100 Trento, Italia, and Cavendish Laboratory, University of Cambridge, United Kingdom.

-
- [1] B. A. Bernevig, T. Hughes, and S. C. Zhang, *Science* **314**, 1757 (2006).
 [2] L. Fu, C. L. Kane, and E. J. Mele, *Phys. Rev. Lett.* **98**, 106803 (2007).
 [3] L. Fu, C. L. Kane, *Phys. Rev. B* **76**, 045302 (2007).
 [4] J. E. Moore, L. Balents, *Phys. Rev. B* **75**, 121306(R) (2007).
 [5] L. Fu, C. L. Kane, *Phys. Rev. Lett.* **100**, 096407 (2008).
 [6] X. L. Qi, T. L. Hughes, and S. C. Zhang, *Phys. Rev. B* **78**, 195424 (2008).
 [7] D. Hsieh *et al.*, *Nature* **452**, 970 (2008).
 [8] D. Hsieh *et al.*, *Science* **323**, 919 (2009).
 [9] Y. Xia *et al.*, *Nat. Phys.* **5**, 398 (2009).
 [10] Y. L. Chen *et al.*, *Science* **325**, 178 (2009).
 [11] P. Roushan *et al.*, *Nature* **460**, 1106 (2009).
 [12] J. L. Zhang *et al.*, arXiv: 1009.3691 (2010).
 [13] C. Zhang *et al.*, arXiv: 1009.3746 (2010).
 [14] D. X. Qu, Y. S. Hor, J. Xiong, R. J. Cava, and N. P. Ong, *Science* **329**, 821 (2010).
 [15] James G. Analytis *et al.*, *Nature Physics* **6**, 960 (2010).
 [16] Z. Ren, A. A. Taskin, S. Sasaki, K. Segawa, and Y. Ando, *Phys. Rev. B*(R) **82**, 241306(R) (2010).
 [17] J. Xiong, A. C. Petersen, D. Qu, Y. S. Hor, R. J. Cava, and N. P. Ong, *Physica E*, *in press*, arXiv:1101.1315 (2011).
 [18] S. Y. Xu *et al.*, arXiv:1007.5111v1 (2010).
 [19] Jun Xiong, Yongkang Luo, YueHaw Khoo, Shuang Jia, R. J. Cava and N. P. Ong, *unpublished*.